

Generalized susceptibility of the magnetic shape-memory alloy Ni₂MnGa

Yongbin Lee, Joo Yull Rhee,* and B. N. Harmon

Ames Laboratory and Department of Physics and Astronomy, Iowa State University, Ames, Iowa 50011

(Received 20 February 2002; published 19 August 2002)

We have investigated the generalized susceptibility $\chi(\mathbf{q})$ and Fermi-surface-nesting of the ferromagnetic shape-memory alloy Ni₂MnGa. As the temperature is lowered below the Curie point, a premartensitic transformation takes place when the magnetization reaches about 84% of its $T=0$ saturated value. We show that the spin-split band structure near this magnetization gives rise in $\chi(\mathbf{q})$ to a prominent peak at $\mathbf{q}=(\frac{1}{3}, \frac{1}{3}, 0)(2\pi/a)$, corresponding to the experimentally observed wave vector for the premartensitic phase.

DOI: 10.1103/PhysRevB.66.054424

PACS number(s): 71.18.+y, 63.20.Dj, 75.50.Cc

The discovery of a martensitic transformation (MT) in ferromagnetic Ni₂MnGa (Ref. 1) has been followed by extensive investigations.²⁻¹⁶ The excitement concerning this alloy stems from the MT giving rise to the shape-memory effect that can be influenced by applied magnetic fields. There are other MT's controlled by magnetism¹⁷ but this one accommodates larger strain and also has a more practical temperature range that can be varied by alloying. This characteristic of Ni₂MnGa means that the shape-memory effect can be better controlled by external magnetic fields as well as temperature for use in sensors and actuators. Ni₂MnGa has a nonmagnetic fcc $L2_1$ Heusler structure with a lattice constant of 5.822 Å at high temperature, and undergoes a ferromagnetic phase transition at 380 K ($\equiv T_C$, the Curie temperature) and a MT to a modulated tetragonal structure having $c/a=0.97$ at 220 K ($\equiv T_M$) upon cooling.¹⁰ T_C and T_M are very sensitive to the atomic ordering and composition of the sample.^{5,11} Additionally, there is a precursor phenomenon related to a premartensitic phase transition for which the atoms are in modulated positions.¹⁰ The modulation has a six-plane period along the [110] direction. At the wave vector $\mathbf{q}=(\zeta, \zeta, 0)(2\pi/a)$ with $\zeta=\frac{1}{3}$, the TA_2 phonon branch of Ni₂MnGa has a strong temperature-dependent dip. Similar premartensitic soft-mode behavior in the same phonon branch has been observed in Ni-Ti (Ref. 18) and Ni-Al (Ref. 19) alloys. In both cases, the phonon softening has been shown to be directly related to Fermi-surface nesting (FSN) and strong electron-phonon coupling.^{20,21} It is natural to ask if the premartensitic phenomenon in Ni₂MnGa is of similar origin.⁴

Since it is well known that the FSN effect can be a driving force for the phonon softening preceding a MT,^{20,21} it would be desirable to investigate the geometry of the Fermi surface. This was the motivation of Velikokhatny and Naumov,¹² who calculated band structures, density of states (DOS), the generalized susceptibility $\chi(\mathbf{q})$, and the Fermi-surface geometry of Ni₂MnGa in both the paramagnetic ($T>T_C$) and ferromagnetic ($T=0$ K) phases. From the results of those calculations, they concluded that the driving force of the premartensitic phonon softening was not related to FSN in the ferromagnetic phase because their calculated nesting vector in the ferromagnetic phase was $\zeta=0.43$, which is substantially larger than the experimental value, $\zeta=\frac{1}{3}$. Rather, they suggested that FSN in the ferromagnetic phase is responsible

for the lattice modulation observed after the MT, resulting in a fivefold modulation along the [110] direction, called the $M(5)$ phase. They also suggested that the premartensitic phase transformation might be caused by anharmonic effects as discussed in Ref. 22.

Since Ni₂MnGa exhibits the shape-memory effect in the ferromagnetic phase, it is desirable to investigate the interplay between the magnetism and the MT and/or phonon softening in this material. The phonon softening persists down to T_M , which is significantly below T_C , but far above $T=0$ K. At $T=T_M$, therefore, the material is not fully magnetized. Since the nesting vector \mathbf{q} could depend on the magnetization, the conclusion of Velikokhatny and Naumov that FSN is not responsible for the phonon softening in the ferromagnetic phase, should be reinvestigated. In this paper we report on the results of calculations of Fermi surfaces and $\chi(\mathbf{q})$ in this partially magnetized region, making use of the Stoner approximation by assuming that the splitting between the majority (spin-up) and minority (spin-down) bands is linearly proportional to the spontaneous magnetization. We find that the nesting vector \mathbf{q} , indeed, depends on the magnetization and that FSN is likely responsible for the phonon softening and premartensitic transformation in the ferromagnetic phase.

We used the scalar relativistic full potential spin-polarized linear muffin-tin orbital method²³ within the local-density approximation with the exchange-correlation potential of Vosko *et al.*²⁴ in these calculations. We used $3d$, $4s$, and $4p$ orbitals for each atomic site for the basis set. To generate the self-consistent potential and charge, we iterated with 47 \mathbf{k} points in the $\frac{1}{48}$ th irreducible Brillouin zone. For the $\chi(\mathbf{q})$ calculations, the whole reciprocal unit cell is divided into $80\times 80\times 80$ parallelepipeds, corresponding to 11 921 irreducible \mathbf{k} points, and each parallelepiped is further cut into six tetrahedra. The \mathbf{k} -space integration was done by using the linear-energy-tetrahedron method.²⁵ For the calculation of $\chi(\mathbf{q})$,

$$\chi(\mathbf{q}) = \sum_{n,m,\mathbf{k}} \frac{f[\epsilon_m(\mathbf{k})]\{1-f[\epsilon_n(\mathbf{k}+\mathbf{q})]\}}{\epsilon_n(\mathbf{k}+\mathbf{q})-\epsilon_m(\mathbf{k})},$$

where $f(\epsilon)$ is the Fermi-Dirac distribution function and $\epsilon_m(\mathbf{k})$ is the m th band energy at \mathbf{k} ; we considered only the bands crossing the Fermi energy (see Table I). Since the results of our $\chi(\mathbf{q})$ calculations for the paramagnetic and

TABLE I. The band numbers for the bands crossing the Fermi level for various magnetizations and temperatures. Temperatures are derived by formulas given in the text.

Magnetization (%)	0	10	30	50	75	100
Temperature (K)	380	379	368	346	293	0
Spin up	20,21	20,21	22-23	22-24	22-24	22-24
Spin down	20,21	19-21	19,20	18-20	18,19	18,19

zero-temperature ferromagnetic phases do not show significant differences with Velikokhatny and Naumov, we will not discuss those results in detail, but will concentrate on the changes in $\chi(\mathbf{q})$ with the magnetization. For calculated magnetic moments, we obtained $3.93\mu_B$ in the unit cell: $3.31\mu_B$ per Mn atom, and $0.31\mu_B$ per Ni atom. These values are consistent with the earlier magnetization measurement¹ and calculated results.^{12,13} Reference 12 contains a good description of the ferromagnetic properties for Ni_2MnGa .

The Stoner theory provides a simple and convenient description for the temperature dependence of the ferromagnetic band structure where we assume that the splitting between the spin-up and spin-down bands is linearly proportional to the magnetization and the permanent spontaneous magnetization follows the relationship given at finite temperature by²⁶

$$M(T) = M_0 f(T),$$

where $M_0 = M(T=0)$, the saturation magnetization at 0 K, and the function $f(T)$ satisfies the equation

$$f(T) = \tanh\left[f(T) \frac{T_C}{T}\right].$$

The function $f(T)$ has solutions of 1 for $T=0$ and 0 for $T=T_C$. This formula is in fairly good agreement with the measured magnetization.⁷ The energy difference between, say, the n th spin-down band and n th spin-up band at any \mathbf{k} point is proportional to the magnetization, and the energy eigenvalues are interpolated as

$$\varepsilon_{\pm}^{\text{ferro}}(n, \mathbf{k}; T \neq 0) = \varepsilon^{\text{para}}(n, \mathbf{k}) - \left[\varepsilon^{\text{para}}(n, \mathbf{k}) - \varepsilon_{\pm}^{\text{ferro}}(n, \mathbf{k}; T=0) \right] \frac{M(T)}{M_0}, \quad (1)$$

where $\varepsilon^{\text{para}}$ ($\varepsilon^{\text{ferro}}$) is the energy eigenvalue with the band index n and \mathbf{k} for the paramagnetic (ferromagnetic) phase, and “+” (“-”) sign corresponds to the spin-up (spin-down) band. We then use the new eigenvalues ($T \neq 0$) to calculate the density of states and obtain the Fermi level and magnetization, which should be the same as the $M(T)$ used in Eq. (1) if the result is self-consistent. We find that at premartensitic transformation temperature ($T_{\text{PM}} \cong 260$ K), the magnetization is about 84% of the full magnetization ($T=0$ K). We note that the above procedure differs from the strict Stoner model in that the band splittings depend on the \mathbf{k} vector. Also, the approximation needs only be reasonable for states near Fermi level for the $\chi(\mathbf{q})$ calculation to be meaningful.

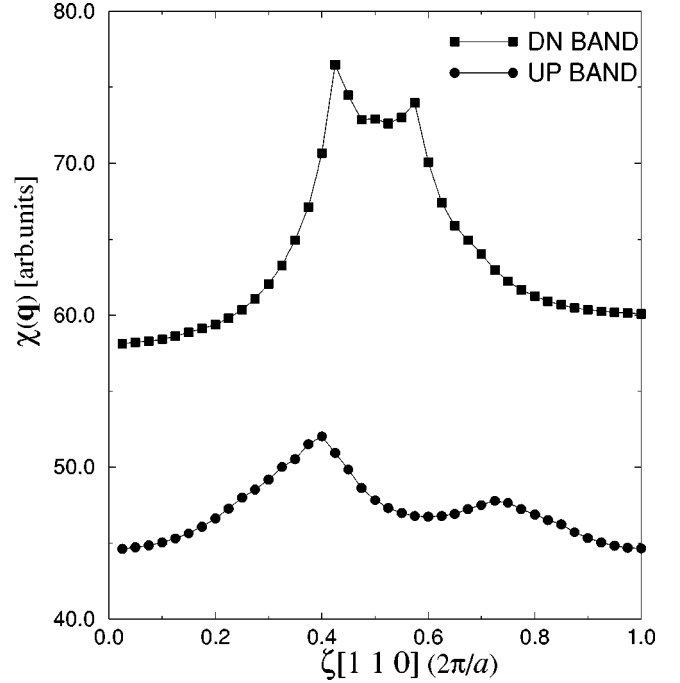


FIG. 1. Total generalized susceptibility contributed by the spin-up and spin-down bands which cross the Fermi level. All solid lines are guides to the eye.

Our calculated band structures (not shown) for both the paramagnetic and ferromagnetic phases are very similar to those previously reported,¹² except the band structure in Ref. 12 contains “ghost” bands (Ga 4d band) above the Fermi level. The calculated DOS is also in good agreement with the DOS reported in Ref. 13. As mentioned previously, the calculated $\chi(\mathbf{q})$'s and Fermi-surface geometry for both the paramagnetic and $T=0$ ferromagnetic phases are very similar to those given in Ref. 12 exhibiting a nesting vector $\mathbf{q} = (\zeta, \zeta, 0)(2\pi/a)$, $\zeta = 0.30(0.425)$ for the paramagnetic (ferromagnetic) phase.

In the fully magnetized case, we have a peak in $\chi(\mathbf{q})$ at $\zeta = 0.425$ (0.40) that arises from the down (up) bands (see Fig. 1). With decreasing magnetization, the peak derived from the down (up) bands moves to larger (smaller) \mathbf{q} values. At 80% magnetization, the peaks are located at $\zeta = 0.5, 0.325$. Worth noting is the nature of the bands which cross the Fermi level. While the up bands (22nd, 23rd, and 24th) have about 0.35 Ry bandwidth, the down bands (18th and 19th) have about 0.07 Ry. Because of smaller dispersion of the spin-down bands, it is likely that temperature effects are more critical for the down bands than for the up bands. The relative magnitudes of the $\chi(\mathbf{q})$ peaks are not indicative of their influence in producing phonon anomalies since the crucial electron-phonon matrix elements have not been included.

The band pair most prominently contributing to the peak at $\zeta = 0.425$ is the 19th spin-down band²⁷ for the fully magnetized case ($T=0$).¹² As the temperature increases from zero, however, the dominant contribution to $\chi(\mathbf{q})$ arises from transitions from states in the 22nd spin-up band to other states in the same band separated by \mathbf{q} . From now on, we

will consider only the 22nd spin-up band, because this band is mostly responsible for FSN in the ferromagnetic phase ($T_M < T < T_C$). Furthermore, we will also consider only the ferromagnetic phase with the magnetization over 60% because of the following three reasons. First, the most dominant contribution comes from the 22nd spin-up band that exhibits a distinct FSN effect. The 22nd spin-up band starts to cross the Fermi level when the magnetization reaches $\sim 30\%$, corresponding to $T = 368$ K, and its contribution to $\chi(\mathbf{q})$ spectrum becomes most significant at 60% magnetization or larger. Second, the phonon softening becomes significant for temperatures below 330 K where the magnetization is 60%. Finally, although the paramagnetic phase has a distinct FSN effect in the 20th band, nesting characteristics of its Fermi surface are somewhat unclear in the magnetization below 60%. We should also remark that when the magnetization is small, the temperature is already high enough to cause considerable smearing of the Fermi surface, so that any FSN would be significantly weakened.

Since the band splitting depends on the magnetization, it is reasonable to expect that the geometry of the Fermi surface and/or the bands crossing the Fermi level can change and thus the FSN vector \mathbf{q} that gives rise to the peak in the $\chi(\mathbf{q})$ spectrum may change. We calculated the $\chi(\mathbf{q})$ and Fermi-surface geometry from the ‘‘adjusted’’ band structures according to Eq. (1). In Table I, the numbers for both spin-up and spin-down bands crossing the Fermi level with various magnetizations and temperatures are listed. The number of bands crossing the Fermi level changes with magnetization. We count the bands above the energy $E = -0.330$ Ry.

The calculated $\chi(\mathbf{q})$ curves with \mathbf{q} along the $[110]$ direction for various magnetizations are shown in Fig. 2, in which only the 22nd spin-up band contribution is shown. There exists a sharp peak around $\zeta = 0.3$ for the magnetization greater than 60%, and the peak moves towards higher ζ as the magnetization increases, or equivalently the temperature decreases. Eventually, ζ reaches the value of 0.4 at full magnetization and is believed to be responsible for the modulated crystal structure, the $M(5)$ phase.¹² According to the results of our calculations, the phonon-softening wave vector \mathbf{q} is changed by the magnetization that can be controlled through the variation of an external magnetic field or by temperature. At 80% magnetization, the nesting vector is $\zeta \cong \frac{1}{3}$, which is the same as the measured one at the transition ($T = 260$ K). This nesting vector is denoted by the arrow in Fig. 3.

Two other important features of Fig. 3 deserve mentioning. The first one is the change of magnitude with magnetization, which can be explained by the geometry of the Fermi surface. As shown in Fig. 3, the area of Fermi surface decreases with increasing magnetization. Since the intensity of $\chi(\mathbf{q})$ depends on the area of nested Fermi surface, the decreasing Fermi-surface area results in the reduction of the intensity of $\chi(\mathbf{q})$. The second one is the change of the width of the peak. The width of the peak decreases as the magnetization increases and reaches its minimum at 80% of full magnetization, and then increases again as the magnetization increases. This is also attributed to the characteristics of the Fermi-surface geometry. As can be seen in Fig. 3, the Fermi surface is completely flattened at $\sim 80\%$ of magnetization,

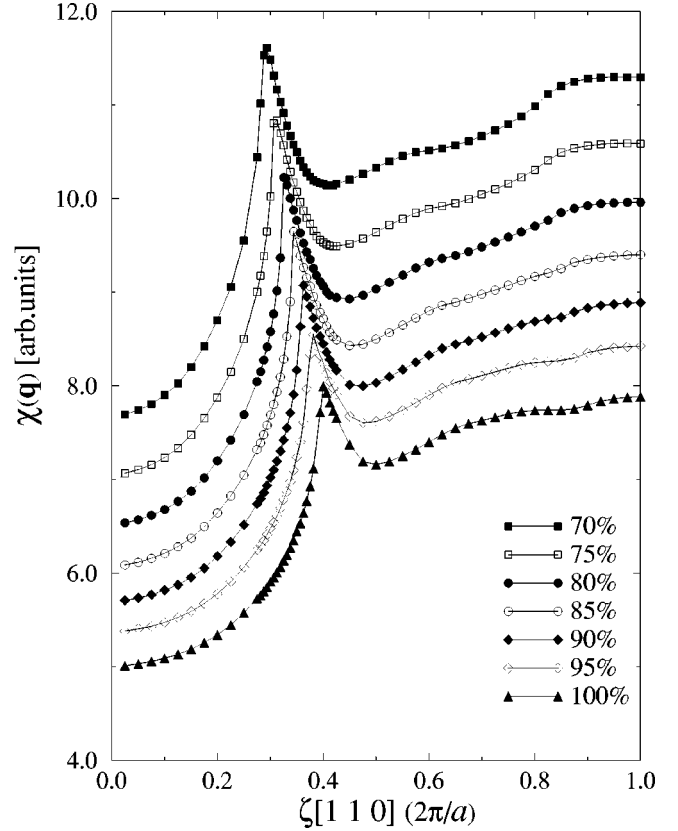


FIG. 2. Magnetization dependence of generalized susceptibility contributed by the 22nd spin-up band. All solid lines are guides to the eye.

while the pair of ‘‘nested’’ bands bends outward (inward) with respect to each other as the magnetization increases (decreases) from 80% magnetization.

The 80% magnetization has special characteristics for the

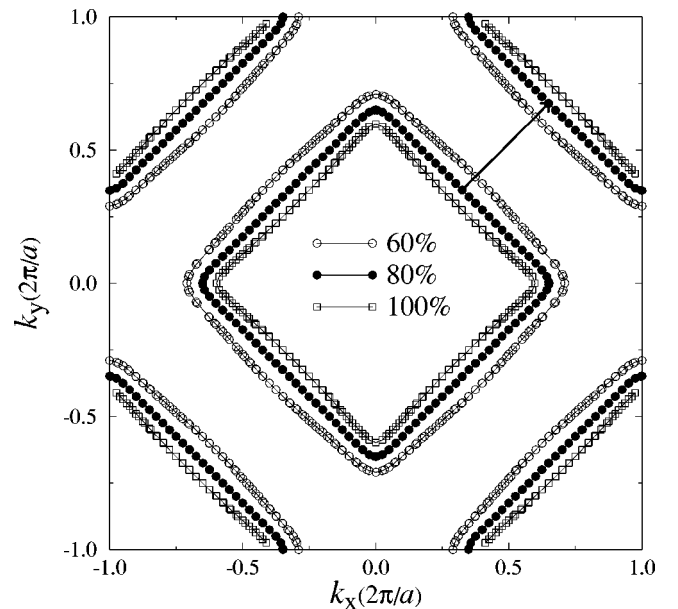


FIG. 3. Fermi surfaces for various magnetizations at $k_z = 0.5$. The nesting vector with $\zeta = \frac{1}{3}$ is denoted by the arrow.

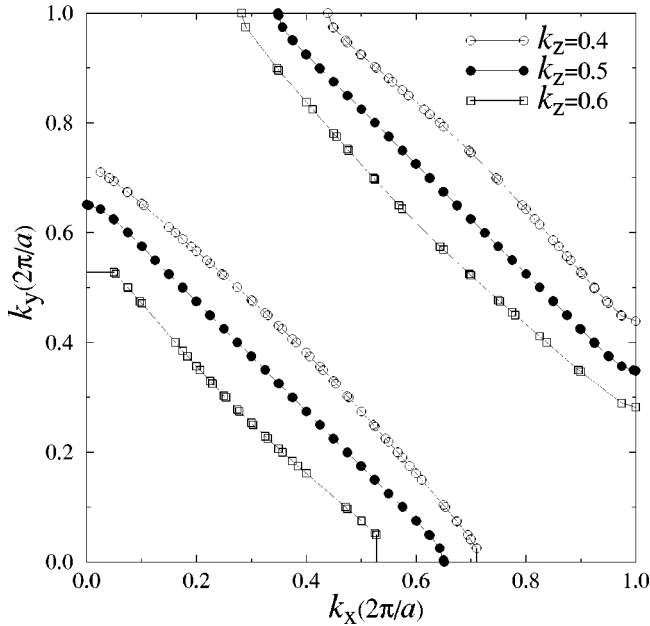


FIG. 4. Geometry of the Fermi surface for various k_z values calculated at 80% magnetization.

phonon softening. At 80% of the magnetization, the FSN is optimized. Not only the Fermi surface is completely flattened in the $k_z=0.5$ plane but the nesting feature persists far from $k_z=0.5$. Figure 4 shows that the Fermi surface intersected the planes perpendicular to the z axis with various k_z values. Although the two sheets of Fermi surface perpendicular to the z direction change their shape appreciably, the parallelism between the two is not altered as k_z changes. Figure 5 shows the Fermi surface in the $[001] \times [110]$ plane. It would seem to have a nesting \mathbf{q} vector that is off the $[110]$ direction. But generalized susceptibility calculations in various directions gave the largest peak in $[110]$ direction. This is related to the curvature of Fermi surface as commented above and shown in Fig. 4. The Fermi surface has different curvatures at different k_z values. The two Fermi surfaces in the nesting region are perfectly nested when they are moved only in the

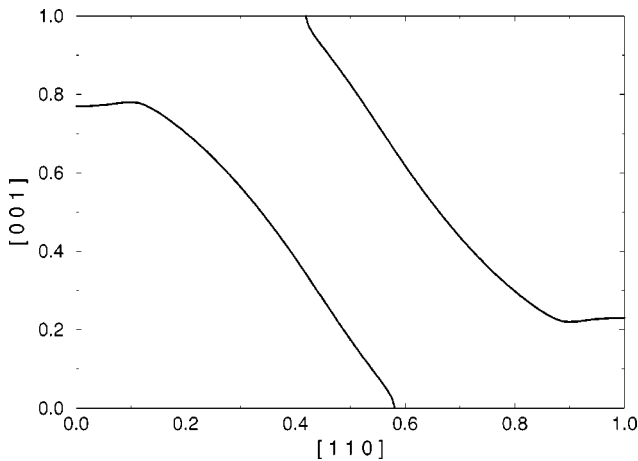


FIG. 5. Geometry of the Fermi surface in the $[001] \times [110]$ plane calculated at 80% magnetization.

$[110]$ direction. Figure 5 does suggest that nesting off the $[110]$ direction will be significant and that phonon softening could extend for some distance off the $(\frac{1}{3}, \frac{1}{3}, 0)$ position.

We did not explicitly evaluate the electron-phonon matrix elements, however, by analyzing the orbital and symmetry properties of the wave functions for those states involved in the FNS, we may deduce that the coupling is strong. The analysis shows the main contribution to the FSN comes from states having predominately Mn character at \mathbf{k} and states with Ni character at $\mathbf{k} + \mathbf{q}$. The Mn states at \mathbf{k} have large d_{xy} , d_{yz} , and d_{zx} components. These components are the diagonal directions of the corresponding planes xy , yz , and zx . The Ni states at $\mathbf{k} + \mathbf{q}$ also have large d_{xy} , d_{yz} , and d_{zx} components. Because these two atoms are located along the body-diagonal direction, the large wave function components of Mn and Ni have what is called a “dormant” symmetry.²⁸ When the atoms are displaced relative to each other along the $[1\bar{1}0]$ direction, this symmetry is broken and large electron-phonon matrix elements result.

There are several studies of the transition temperature changes with different electron concentrations^{16,29–31} and magnetic fields.^{6,7,32} And recently, L. Mañosa *et al.*³³ reported that the location of the dip in $[110]$ TA_2 phonon branch can be changed by altering the electron concentration. A rigid band model using our band structure can explain reasonably well the effects of electron concentration, but the energy scale is completely different for understanding the magnetic-field effects on the \mathbf{q} vector if band splitting is the only thing considered. We believe that domain structure and magnetoelastic coupling must also be considered.

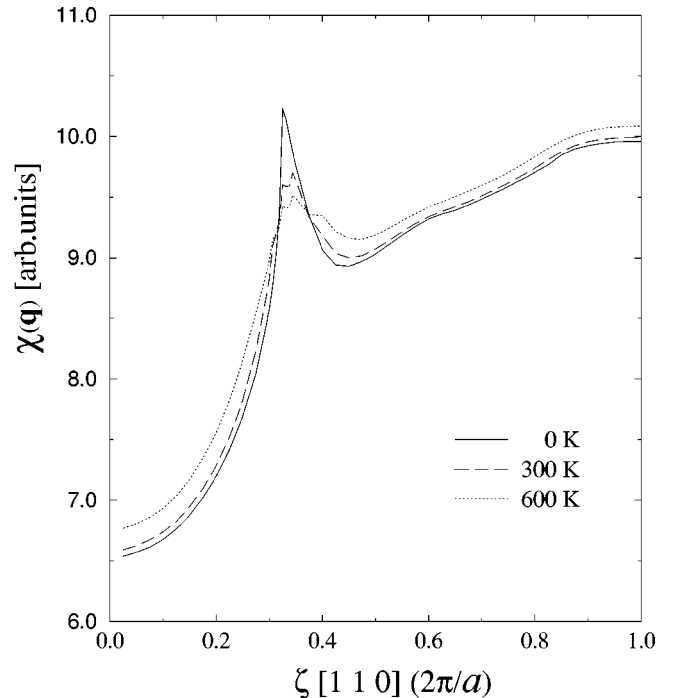


FIG. 6. The generalized susceptibility $\chi(\mathbf{q})$, evaluated using Fermi-Dirac distribution for 0 K, 300 K, and 600 K with the energy bands split for 80% magnetization (corresponding to ≈ 270 K).

Until now, we assumed $T=0$ for the Fermi-Dirac distribution function $f(\epsilon)$,

$$f(\epsilon) = \begin{cases} 1 & \text{if } \epsilon < \epsilon_F \\ 0 & \text{if } \epsilon > \epsilon_F. \end{cases}$$

However, because temperature affects the Fermi surface by changing the distribution as well as the band splitting, it is worth commenting on the change in $\chi(\mathbf{q})$ caused by finite temperature changes of the Fermi-Dirac distribution function. Figure 6 shows the $\chi(\mathbf{q})$ with the Fermi-Dirac distribution function evaluated at three different temperatures using the bands at 80% magnetization. The sharp peak in $\chi(\mathbf{q})$ is still present, but rounded by the thermal distribution effects. It is an expected result.

In summary, we have presented computational results for the generalized susceptibility $\chi(\mathbf{q})$ and the geometry of the Fermi surface for Ni_2MnGa with various magnetizations. A peak of the $\chi(\zeta, \zeta, 0)$ curve is related to FSN and moves toward higher ζ values as the magnetization develops. Furthermore, the geometry of the spin-up Fermi surface is closely related to the intensity and width of the peak as well as the peak position in the $\chi(\mathbf{q})$ spectrum. The Fermi-surface nesting effect is optimized at 80% of full magnetization and the nesting \mathbf{q} vector at 80% magnetization is exactly the same as that of the observed phonon softening, $\zeta = \frac{1}{3}$. The

80% magnetization occurs close to the temperature region near which the premartensitic transformation occurs. These results strongly suggest that the Fermi-surface nesting is a dominant driving force for the phonon softening in the ferromagnetic phase down to the temperature where the premartensitic structural phase transition occurs. Thus, similar to the phenomena observed in Ni-Ti and Ni-Al alloys, Fermi-surface nesting along with strong electron-phonon coupling leads to a dramatic temperature-dependent softening of particular phonon modes. These modes are responsible for the observed premartensitic phase transformation. Whether the premartensitic transformation (static displacements) is realized or not, it is believed that the softening of the phonon modes (dynamic) can lower the relevant energy barrier and promote the low-temperature martensitic transformation.³⁴

Highly precise measurement of the wave vector for the premartensitic phase in high magnetic fields might confirm the above picture of magnetic Fermi-surface nesting. Such experiments may be inconclusive if lattice strain energies are strong enough to suppress incommensurate ordering near the $(\frac{1}{3}, \frac{1}{3}, 0)$ wave vector. High-pressure experiments may offer an alternative approach if high precision can be attained.

The Ames Laboratory is operated for the US Department of Energy by the Iowa State University under Contract No. W-7405-Eng-82. One of us (J.Y.R.) was also supported by the Korea Research Foundation Grant No. KRF-01-DP0193.

*Permanent address: Department of Physics, Hoseo University, Asan, Choongnam 336-795, Korea.

¹P.J. Webster, K.R.A. Ziebeck, S.L. Town, and M.S. Peak, *Philos. Mag. B* **49**, 295 (1984).

²S. Fujii, S. Ishida, and S. Asano, *J. Phys. Soc. Jpn.* **58**, 3657 (1989).

³G. Fritsch, V.V. Kokorin, and A. Kempf, *J. Phys.: Condens. Matter* **6**, L107 (1994).

⁴A. Zheludev, S.M. Shapiro, P. Wochner, A. Schwartz, M. Wall, and L.E. Tanner, *Phys. Rev. B* **51**, 11 310 (1995).

⁵U. Stuhr, P. Vorderwisch, V.V. Kokorin, and P.-A. Lindgård, *Phys. Rev. B* **56**, 14 360 (1997).

⁶A. Planes, E. Obradó, A. González-Comas, and L. Mañosa, *Phys. Rev. Lett.* **79**, 3926 (1997).

⁷F. Zuo, X. Su, and K.H. Wu, *Phys. Rev. B* **58**, 11 127 (1998).

⁸A. González-Comas, E. Obradó, L. Mañosa, A. Planes, V.A. Chernenko, B.J. Hattink, and A. Labarta, *Phys. Rev. B* **60**, 7085 (1999).

⁹P.J. Brown, A.Y. Bargawi, J. Crangle, K.-U. Neumann, and K.R.A. Ziebeck, *J. Phys.: Condens. Matter* **11**, 4715 (1999).

¹⁰A. Zheludev, S.M. Shapiro, P. Wochner, and L.E. Tanner, *Phys. Rev. B* **54**, 15 045 (1996).

¹¹For the compilation of the experimental results for various samples, see, for example, T. Castan, E. Vives, and P.-A. Lindgård, *Phys. Rev. B* **60**, 7071 (1999).

¹²O.I. Velikokhatny and I.I. Naumov, *Phys. Solid State* **41**, 617 (1999). The band structure in this paper contains the so-called “ghost bands” arising from Ga 4d states (compare with Ref.

13). Since they occur above the Fermi level they do not significantly influence the Fermi surface.

¹³M. Pugaczowa-Michalska, *Acta Phys. Pol. A* **96**, 467 (1999).

¹⁴A. Zheludev and S.M. Shapiro, *Solid State Commun.* **98**, 35 (1996).

¹⁵T. Kanomata, K. Shirakawa, and T. Kaneko, *J. Magn. Magn. Mater.* **65**, 76 (1987).

¹⁶A.N. Vasil'ev, A.D. Bozhko, V.V. Khovailo, I.E. Dikshstein, V.G. Shavrov, V.D. Buchelnikov, M. Matsumoto, S. Suzuki, T. Takagi, and J. Tani, *Phys. Rev. B* **59**, 1113 (1999).

¹⁷T. Kakeshita and K. Shimizu, *Trans. Mater. Res. Soc. Jpn.* **18B**, 981 (1994).

¹⁸S.K. Satija and S.M. Shapiro, *Phys. Rev. B* **29**, 6031 (1984).

¹⁹S.M. Shapiro, J.Z. Larese, Y. Noda, S.C. Moss, and L.E. Tanner, *Phys. Rev. Lett.* **57**, 3199 (1986).

²⁰G.L. Zhao and B.N. Harmon, *Phys. Rev. B* **45**, 2818 (1992).

²¹G.L. Zhao and B.N. Harmon, *Phys. Rev. B* **48**, 2031 (1993).

²²R.J. Gooding and J.A. Krumhansl, *Phys. Rev. B* **39**, 1535 (1989).

²³S.Yu. Savrasov and D.Yu. Savrasov, *Phys. Rev. B* **46**, 12 181 (1992).

²⁴S.H. Vosko, L. Wilk, and M. Nussair, *Can. J. Phys.* **58**, 1200 (1980).

²⁵J. Rath and A.J. Freeman, *Phys. Rev. B* **11**, 2109 (1975).

²⁶See, for example, H. Ibach and H. Lüth, *Solid-State Physics*, 2nd ed. (Springer, Berlin, 1995), pp. 169–172.

²⁷The band index in Ref. 12 is smaller than ours by 5 because we treat the Ga 3d bands as valence states.

²⁸W. Weber, in *The Electronic Structure of Complex System*, edited

- by P. Phariseau and W. M. Temmerman (Plenum Press, New York, 1984).
- ²⁹A.D. Bozhko *et al.*, Zh. Eksp. Teor. Fiz. **115**, 1740 (1999) [JETP **88**, 954 (1999)].
- ³⁰F. Zuo *et al.*, J. Phys.: Condens. Matter **11**, 2821 (1999).
- ³¹V.V. Khovailo *et al.*, J. Phys.: Condens. Matter **13**, 9655 (2001).
- ³²W.H. Wang *et al.*, J. Phys.: Condens. Matter **13**, 2607 (2001).
- ³³L. Mañosa *et al.*, Phys. Rev. B **64**, 024305 (2001).
- ³⁴J.A. Krumhansl and R.J. Gooding, Phys. Rev. B **39**, 3047 (1989).